Neutral Associated Production by 8-, 10.7-, and 15.7-GeV/c π^- Incident on Protons*

K. J. Foley, W. A. Love, S. Ozaki, E. D. Platner, A. C. Saulys, and E. H. Willen
Brookhaven National Laboratory, Upton, New York 11973

S. J. Lindenbaum
Brookhaven National Laboratory, Upton, New York 11973
City College of the City University of New York, New York, New York 10031
(Received 12 February 1973)

We present differential and total cross sections for two reactions: $\pi^- p \to K^0\Lambda$ and $\pi^- p \to K^0\Sigma^0$. The incident pion momenta were 8, 10.7, and 15.7 GeV/c. The results are based on an analysis of approximately 22 600 events of the two reactions where the π^+ and π^- from the decay of the K_S^0 were detected in the forward leg of the Double Vee Magnetic Spectrometer. The separation of Λ recoils from Σ^0 recoils was accomplished by the missing-mass technique.

I. INTRODUCTION

There have been numerous measurements of the associated production reactions

$$\pi^- p \to K^0\Lambda, \tag{1}$$

$$\pi^- p \to K^0\Sigma^0. \tag{2}$$

The measurements which have been able to separate Λ and Σ^0 production have been bubble-chamber measurements at lower momentum.[1] Spark-chamber and counter measurements[2] have been made at higher momentum, but with insufficient resolution to isolate the two processes. The motivation for separating reactions (1) and (2) was to obtain the individual behavior of the cross sections as functions of s and t, which might be quite different from the behavior of the combined cross sections. These separated reactions are much more useful for checking the predictions of various models.[3]

Preliminary results from some of these data have been presented earlier.[4] Of course, the results presented here supersede any preliminary presentation.

II. APPARATUS AND EXPERIMENTAL PROCEDURE

The beam used for this experiment was an unseparated secondary negative beam produced at 0° at target station A by the slow extracted beam from the Brookhaven AGS (see Fig. 1). Two scintillation counter hodoscopes $H2$ and $H3$ were used to measure the angle of incidence at the hydrogen target to ±0.25 mrad (rms) while a third hodoscope $H1$ upstream of a set of three bending magnets $D3$, $D4$, $D5$ (8.7° total bend) permitted the incident momentum to be determined to ±0.2%. Each hodoscope used 16 horizontal and 16 vertical scintillators $2\frac{1}{4}$ in. by $\frac{1}{8}$ in. by $\frac{1}{16}$ in. thick. Threshold Čerenkov counters $CT1$ and $CT2$ were used to select pions in the incident beam.

In this experiment we detected the pions from the decay of K_S^0 emitted in the forward direction and separated reactions (1) and (2) by the missing-mass technique. The apparatus, shown in Fig. 2, is the forward arm of the BNL Double Vee Spectrometer, which is described in detail elsewhere.[5] Briefly, the apparatus is a high-resolution, magnetic spectrometer using low-mass, aluminum-wire spark chambers with magnetostrictive readout in front of and behind a 48D48 bending magnet. The magnet aperture is 48 in. wide by 48 in. long by 18 in. high with 16.5-kG central field. The size of the active area of the spark chambers varied from 1 ft by 3 ft for the smallest chamber to 4 ft by 13 ft for the largest. All but two of the spark-chamber modules (S.C.) shown in Fig. 2 consisted of two gaps of vertical wires measuring the x coordinate, two gaps of horizontal wires measuring the y coordinate, and one of "w" wires at 45° to x and y. The first module contained an extra set of x and y gaps, and the last module contained no w gap. The wires on opposite sides of each gap were made parallel to improve the multiparticle efficiency of the system. Each wire plane was read out and the two readings from each gap were averaged to give the position of the spark in the gap. With this technique a spatial resolution of approximately 0.2 mm was obtained. Up to eight sparks could be encoded for each readout. In order to minimize biases in the apparatus acceptance, the beam area of the chambers was not deadened. The angular resolution varied from 0.4 mrad at 4 GeV/c to 0.15 mrad at 20 GeV/c. The momentum resolution varied from 0.4% at 4 GeV/c to 0.6% at 20 GeV/c. The liquid-hydrogen target had a cylindrical cell 2 ft long and 4 in. in diameter with

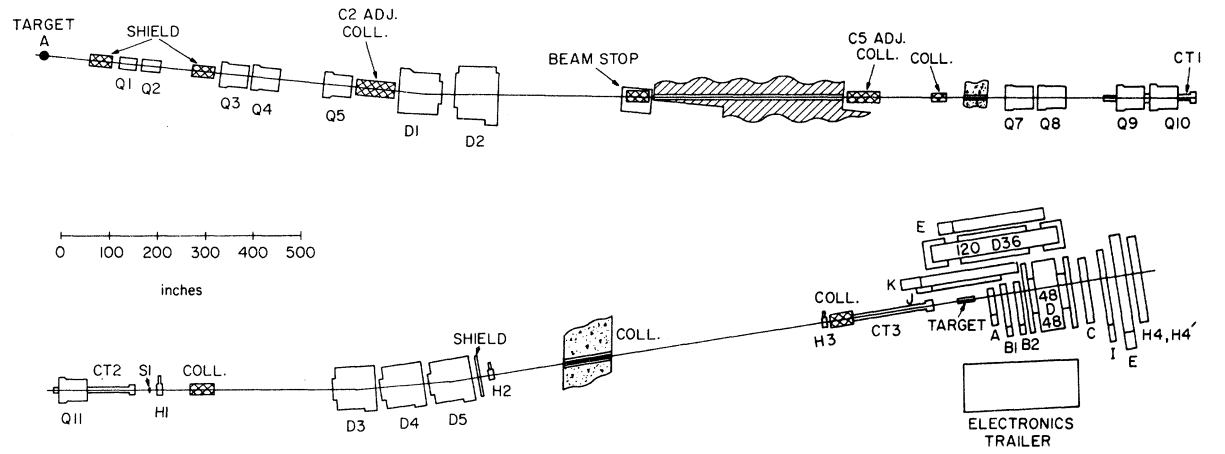

FIG. 1. The layout of the beam to the BNL Double Vee Magnetic Spectrometer. Because of the length of the beam, the figure has been divided in two between quadrupoles Q10 and Q11.

0.0075-in.-thick Mylar walls capped with 0.005-in.-thick Mylar domes. This cell was located in a vacuum box with an incident beam port (0.005 in. Mylar) and a 0.014-in.-thick Mylar window covering the forward direction and the sides. Forty layers of aluminized Mylar superinsulation (0.01 in. total thickness) were wrapped around the cell. Scintillation counter A, $\frac{1}{8}$ in. thick by 8 in. high by 14 in. wide, was placed 2.7 in. from the downstream end of the liquid-hydrogen target. Scintillation counter B was $\frac{1}{8}$ in. thick by 13 in. high by 30 in. wide, viewed by four phototubes, and located behind the first spark-chamber module. $H4$ and $H4'$ were hodoscopes of scintillators viewed by two phototubes each. $H4$ had 64 elements, each 0.5 in. thick by 2.5 in. wide by 45 in. long; $H4'$ had 17 elements, each 0.5 in. thick by 10 in. wide by 54 in. long.

The event topology of interest was a neutral particle emerging from the target in the forward direction and decaying into two charged particles in the region between the counters A and B, both particles passing through the 48D48 magnet aperture and reaching the hodoscopes $H4$ and $H4'$. The trigger system for selecting this topology was

$$S1 \cdot H1 \cdot H2 \cdot H3 \cdot \overline{M} \cdot \overline{A} \cdot B \cdot [(H4 \geq 2) \cdot (H4' \geq 2)],$$

where $\overline{M}$ indicates that an event was rejected if more than one counter was fired in any of the six screens of $H1$, $H2$, $H3$, and where $[(H4 \geq 2) \cdot (H4' \geq 2)]$ refers to two or more signals in $H4'$ correlated with signals in $H4$ that could have been produced by particles emerging from the magnet aperture. The trigger rate varied from 3×10^{-5} per incident beam particle at 8 GeV/c to 8×10^{-5} at 15.7 GeV/c. We included one event per AGS pulse which was a trigger requiring only an incident beam particle and was used to monitor the beam momentum.

The data were recorded on magnetic tape and transmitted in parallel to the PDP-10 computer of the BNL On-Line Data Facility. The computer did complete on-line analysis of about 10–25% of the events in order to give continuous information on the spectrometer performance for real events, the K^0 mass resolution, the recoil mass spectrum, etc. In addition, the computer monitored the output of a fast-cycling digital voltmeter (16 readings per AGS pulse) which stepped sequentially through the various magnet shunt voltages, magnet Hall voltages and currents, high-voltage supply outputs, etc. The computer was programmed to type out a warning when any reading deviated from the set value by more than the preset tolerance (typically 1% for quadrupole magnets and 0.1% for the dipole magnets).

III. DATA ANALYSIS AND RESULTS

A. Pattern Recognition

The off-line analysis was performed on the BNL CDC 6600 computers. The major computing task

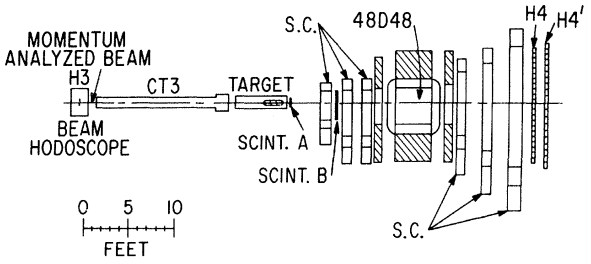

FIG. 2. The detection apparatus for this experiment. The labels S.C. indicate the spark-chamber modules. The individual components are described in the text.

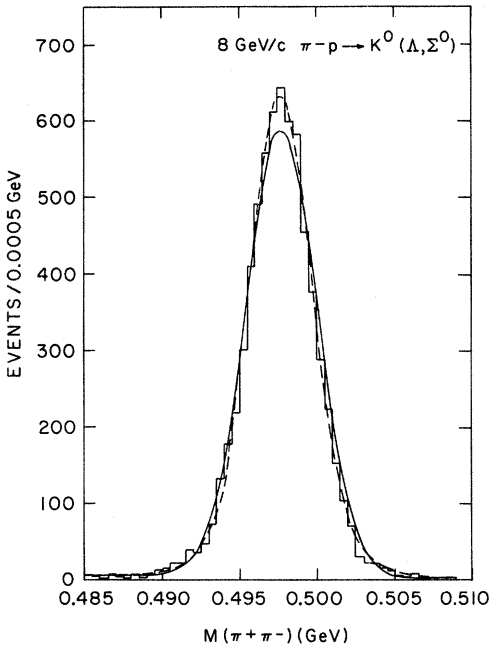

FIG. 3. The $\pi^+\pi^-$ effective-mass spectrum in the K^0 mass region for the events at 8 GeV/c incident momentum. The half width at half maximum (hwhm) of the dashed curve (the curves are described in the text) is 2.4 MeV.

was the pattern recognition problem of combining the spark coordinates into track segments. The technique used was to treat each two-dimensional "view" of the event separately and to look for straight-line segments containing at least four sparks. The "x view" and "y view" tracks thus found were combined into three-dimensional tracks by checking which combinations coincided with the sparks observed in the w planes (oriented at 45° to the x and y directions); then the track segments were connected through the magnet. The momentum of each particle was calculated using a polynomial representation of the magnetic field length integral as a function of the incident angle, position, and approximate momentum of the track. (The approximate momentum was calculated assuming a uniform field.) Tracks which did not intersect triggered counters in the $H4$ hodoscope were ignored. Among the remaining tracks, three-dimensional vertices were sought downstream of counter A. If the event contained a neutral vee decaying between counters A and B, the momentum and positions of the tracks were written on a data summary tape which was used for subsequent analysis. This criterion was met by 6% of the triggers at 8 GeV/c and by 14% of the triggers at 15.7 GeV/c. About 90% of these neutral vees had an effective mass corresponding to the K^0 meson.

B. Resolution Function

The K^0 mass spectrum for the 8-GeV/c data is shown in Fig. 3. Owing to effects such as scattering in the spark chambers, δ-ray production, and decay of the pion in the spectrometer, we expect the over-all resolution function to be approximately, but not exactly, Gaussian. The solid curve in Fig. 3 is a Gaussian fit to the data. The shape is not quite correct, particularly in the tails. However, because of the high statistics obtained in this experiment, we need to have a good representation of the resolution function if χ^2 is to be useful in determining fits to the data; a good fit is obtained using a functional form constructed by adding a second, somewhat wider Gaussian term. This is shown as a dashed curve in Fig. 3. Clearly the deviation from a Gaussian shape is small. Figure 4 shows the momentum resolution of the spectrometer for 10-GeV/c pions. Again, the solid curve is the best Gaussian fit while the dashed curve is the sum of two Gaussians. In both spectra we find that a good fit can be obtained over a fairly wide range for the ratio of the widths. The same technique was used for fitting the peaks in the missing-mass-squared spectra.

C. Kinematic Analysis and Fitting

In order to have well-defined detection efficiency we cut the data sample, including only events with

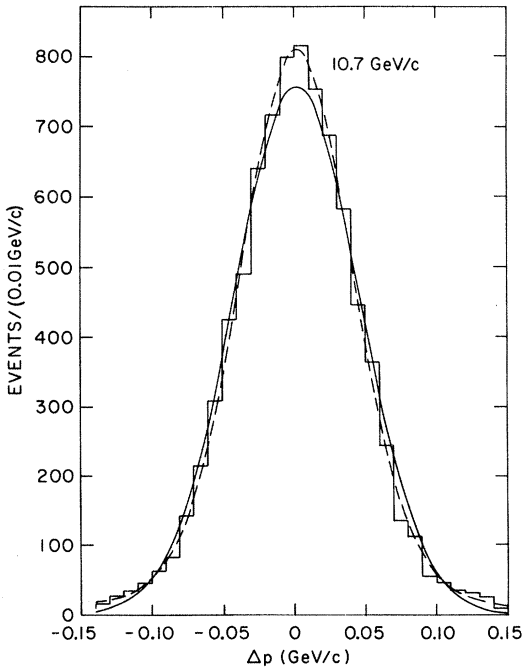

FIG. 4. Momentum resolution for 10.7-GeV/c particles analyzed in the forward spectrometer. The half width at half maximum of the dashed curve is 47 MeV/c.

decay vertices between counter A and the first spark-chamber module (14.7 in. to 47 in. from the center of the hydrogen target) and with both tracks passing through a well-defined magnet aperture and having momentum greater than 1.2 GeV/c. The $\pi^+\pi^-$ effective-mass distribution for the 8-GeV/c final data sample is shown in Fig. 3. The peak at 0.4977 GeV is in excellent agreement with the accepted K^0 mass. Since Λ hyperons also satisfy the trigger topology, all neutral vees were reanalyzed assuming that the decay products were a proton and a negative pion. About 4% of the vees are Λ decays but, due to the kinematic constraints, the contamination of the K^0 sample by Λ's is negligible. We estimate the non-K^0 background in our K^0 sample to be about 1% at each momentum. The $\pi^+\pi^-$ effective mass was not constrained in the fitting of the events.

The missing-mass-squared spectra were histogrammed for all the data at the various incident momenta (Figs. 5–7). Also, at each momentum, histograms of the same spectrum were made up for various intervals of $t' = t - t_{\min}$ (where t is the negative of the four-momentum transfer squared). In order to determine the shape and width of the Λ and Σ^0 peaks in the missing-mass-squared spectrum, we first did a maximum-likelihood fit at each momentum to all the data in the Λ, Σ^0 region. The following free parameters were used in the fits:

(1) the width of the narrower Gaussian,
(2) the ratio of the widths of the two Gaussians,
(3) the ratio of the amplitudes of the two Gaussians,
(4) the square of the Λ mass,
(5) the square of the Σ^0 mass,
(6) the ratio of the Σ^0 to the Λ amplitude, and
(7) the amplitude of a linear background commencing at 1.45 GeV^2 (i.e., the $\Lambda\pi$ threshold lowered by 0.13 GeV^2 for resolution).

The Λ and Σ^0 masses were made variable to allow for small shifts in the absolute mass scale. In the worst case (at 15.7 GeV/c) the Σ^0 mass came out 3.2 MeV high relative to the Λ mass.[6] This procedure worked very well at 8 and 10.7 GeV/c where the Λ and Σ^0 peaks are seen to be separated in the missing-mass-squared plots. At 15.7 GeV/c separation is poor and the parameters of the two Gaussian resolution functions were poorly determined. Therefore, the 15.7-GeV/c data were fitted with a Gaussian resolution function. The solid lines in Figs. 5–7 show the over-all fit to the spectrum and the contribution from each term (Λ,

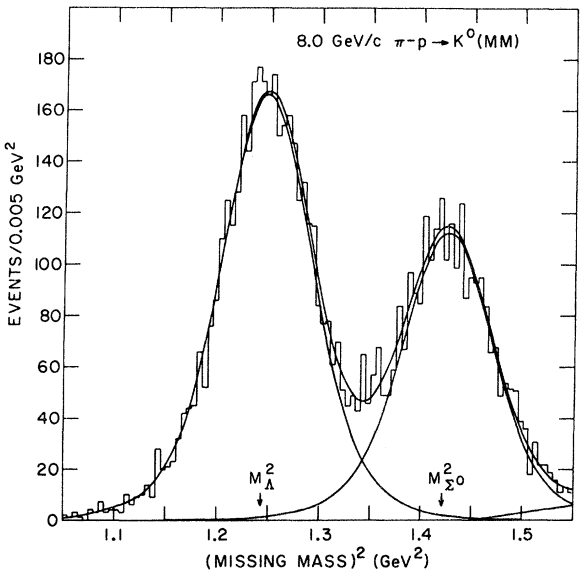

FIG. 5. Number of events plotted versus the square of the missing mass from the K^0 for the 8-GeV/c data. The histogram is the raw data uncorrected for spectrometer acceptance. The curves are the fits described in the text with the Λ, Σ^0, and background contributions shown separately. The half width at half maximum of the resolution curve is 0.052 GeV^2 corresponding to a missing-mass resolution of 23 MeV at the Λ mass. The fit is good, i.e., $\chi^2 = 98.2$ for 92 degrees of freedom. The separation of Λ events and Σ^0 events is excellent.

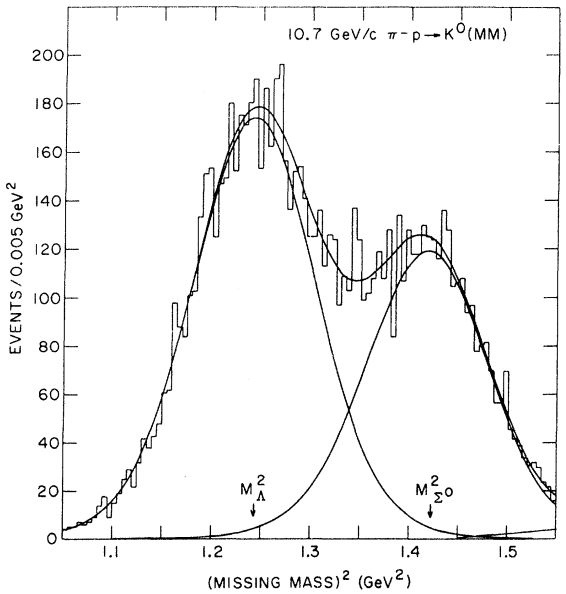

FIG. 6. Number of events plotted versus the square of the missing mass from the K^0 for the 10.7-GeV/c data. The curves are the fits described in the text with the Λ, Σ^0, and background contributions shown separately. The half width at half maximum of the resolution curve is 0.073 GeV^2 which corresponds to a missing-mass resolution of 33 MeV at the Λ mass. The fit gives $\chi^2 = 95.3$ for 92 degrees of freedom. The separation of Λ events and Σ^0 events is good.

Σ^0, and background).

For the fits to the data in the individual t' bins, all parameters except Nos. 6 and 7 were fixed at the best values from the over-all fit. The fitted Λ and Σ^0 mass peaks were then integrated to obtain the number of events of each reaction in each t' bin.

D. Corrections to the Data

The measured event rate was corrected for each of the following effects:

(1) the two-charged-pion decay branching ratio of the K^0 (0.344),

(2) empty-target background (3.3%),

(3) nuclear attenuation in the hydrogen target and spectrometer counters (6%),

(4) electron[7] and muon contamination in the incident beam (5–10%),

(5) inefficiency of the trigger system (5%),

(6) event detection inefficiency[8] (10–15%),

(7) pion decay in the spectrometer (3–6%), and

(8) acceptance of the apparatus.

E. Acceptance Calculation

The acceptance of the apparatus for both reactions (1) and (2) was calculated as a function of t' by a Monte Carlo program. The calculations took into account the momentum, angle, and spatial distributions of the incident beam as well as the geometric cuts applied to the data. Interaction points were generated at random along the length of the liquid-hydrogen target. An exponential approximation was used to represent the t' dependence. The reaction products were then followed through the apparatus and tests were made for various effects that could lose events. For about 60% of the generated events, the K^0 decay point is upstream of the veto counter A. Large $|t|$ events tend to be lost more than small $|t|$ events due to the finite apertures of the 48D48 magnet. Very few events are lost due to the sizes of the hodoscopes and spark chambers. Some events are lost because the opening angle of the two pions from the decay of the K^0, projected onto the xz or yz planes (the incident beam axis is the z direction), is too small to be resolved by the spark chambers or by the reconstruction programs; cutoffs of 4 mrad for both the xz and yz projections were used in the Monte Carlo program for these effects. Events with particles having momenta smaller than 1.2 GeV/c were eliminated from the data and from the Monte Carlo calculation. Events in which a particle struck the $H4$ hodoscope counters in the beam region were lost, as the signals from these counters were removed from the trigger. Events were lost whenever the recoil decay products triggered counter A. Estimation of this effect required that the decay of the recoil particle in the reaction under consideration be simulated, including its decay point in the target and the passage of its decay products through liquid hydrogen to reach counter A. In the reactions under consideration, this effect tends to remove more events at small $|t|$ and is largely independent of the polarization of the recoil particle. The over-all acceptances for the apparatus (Fig. 8) are steep but smooth functions of t.

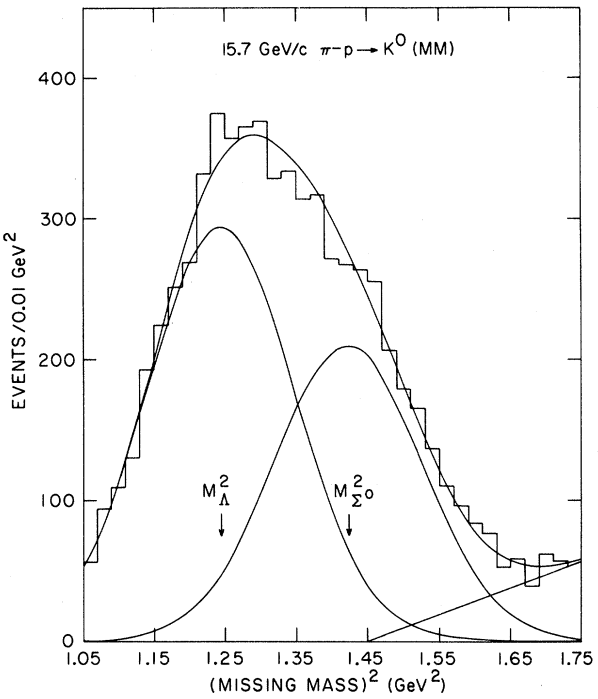

FIG. 7. Number of events plotted versus the square of the missing mass from the K^0 for the 15.7-GeV/c data. The curves are the fits described in the text with the Λ, Σ^0, and background contributions shown separately. Here no dip is seen between the Λ and Σ^0 events, but a separation is still possible. The resolution is 0.123 GeV^2 (hwhm) corresponding to a missing-mass resolution of 55 MeV at the Λ mass. The fit χ^2 is 29.4 for 31 degrees of freedom.

F. Cross-Section Results

The cross sections obtained after all corrections were applied are listed in Table I and shown in Figs. 9–12. The errors shown include counting statistics and, for the cross sections of the individual reactions, a contribution due to the uncertainty in the fitting procedure.

G. Systematic Uncertainties

In addition to counting statistics, the following sources of uncertainty in the measurement must

be taken into account:

(1) efficiency of the trigger system (5%),
(2) event reconstruction efficiency (±5%),
(3) acceptance calculation (±5%) (the largest uncertainty is in the calculation of how often the decay products of the recoil Λ or Σ^0 trigger the veto counter A),
(4) electron and muon contamination of the beam (±3%), and
(5) pion decays in the spectrometer (±2%).

As a result, we estimate about 10% scale uncertainty in any absolute cross section given. Of this, we estimate about half is momentum-dependent.

At 15.7 GeV/c the resolution is insufficient to separate the Λ and Σ^0 peaks clearly on the missing-mass-squared plot. As a result of this, we have added 0.10 to the error of the ratio of Λ to Σ^0 and the individual cross sections for reactions (1) and (2) are subject to a scale error of 15% at 15.7 GeV/c.

We estimate that the t-dependent systematic errors are $\lesssim 5\%$ and thus are smaller than the statistical errors on most of the measured points.

TABLE I. Differential cross section for reaction (1) ($\pi^- p \to K^0\Lambda$) and (2) ($\pi^- p \to K^0\Sigma^0$) and the sum of the two, (a) at 8.0 GeV/c, (b) at 10.7 GeV/c, and (c) at 15.7 GeV/c. In addition to the errors in the table (chiefly counting statistics), there is an over-all systematic scale uncertainty of ±10% for (a) and (b) and 15% for (c) as described in the text.

t' Range [(GeV/c)^2]		$\pi^- p \to K^0\Lambda$ [μb/(GeV/c)^2]	$\pi^- p \to K^0\Sigma^0$ [μb/(GeV/c)^2]	$\pi^- p \to K^0 Y^0$ [μb/(GeV/c)^2]
		(a) $P_{\text{beam}} = 8.0$ GeV/c		
0 to	−0.05	131.0 ± 3.1	114.3 ± 3.2	245.3 ± 4.2
−0.05	−0.10	90.5 ± 3.1	73.3 ± 3.0	163.8 ± 4.1
−0.1	−0.15	70.2 ± 3.3	45.5 ± 3.0	115.7 ± 4.2
−0.15	−0.2	46.9 ± 2.8	33.8 ± 2.4	80.6 ± 4.2
−0.2	−0.25	30.9 ± 3.1	17.3 ± 2.5	48.1 ± 3.7
−0.25	−0.3	23.1 ± 2.8	9.5 ± 2.2	32.6 ± 3.3
−0.3	−0.4	10.3 ± 1.4	5.5 ± 1.1	15.9 ± 1.7
−0.4	−0.5	7.2 ± 1.4	3.1 ± 1.0	10.3 ± 1.6
−0.5	−0.6	4.9 ± 1.4	3.5 ± 1.2	8.4 ± 1.7
−0.6	−0.8	0.91 ± 0.43	1.2 ± 0.5	2.2 ± 0.6
−0.8	−1.0	0.18 ± 0.51	2.7 ± 1.1	2.9 ± 1.1
		(b) $P_{\text{beam}} = 10.7$ GeV/c		
0	−0.05	97.8 ± 2.2	82.9 ± 2.2	180.7 ± 2.8
−0.05	−0.10	64.7 ± 1.8	49.4 ± 1.6	114.1 ± 2.4
−0.1	−0.15	41.8 ± 1.7	30.4 ± 1.5	72.2 ± 2.1
−0.15	−0.2	29.5 ± 1.6	19.5 ± 1.4	48.9 ± 1.9
−0.2	−0.25	17.8 ± 1.3	12.3 ± 1.2	30.2 ± 1.7
−0.25	−0.3	14.8 ± 1.4	9.4 ± 1.2	24.2 ± 1.7
−0.3	−0.4	9.16 ± 0.88	4.17 ± 0.72	13.3 ± 1.0
−0.4	−0.5	4.94 ± 0.78	1.91 ± 0.57	6.86 ± 0.89
−0.5	−0.6	3.51 ± 0.78	0.93 ± 0.47	4.44 ± 0.85
−0.6	−0.8	1.66 ± 0.42	0.68 ± 0.32	2.35 ± 0.45
−0.8	−1.0	1.57 ± 0.40	0.03 ± 0.16	1.60 ± 0.38
		(c) $P_{\text{beam}} = 15.7$ GeV/c		
0	−0.025	65.1 ± 3.1	53.6 ± 3.2	118.7 ± 3.3
−0.025	−0.05	56.1 ± 2.9	51.3 ± 3.0	107.4 ± 3.1
−0.05	−0.1	37.4 ± 1.7	30.5 ± 1.7	67.9 ± 1.7
−0.1	−0.15	25.6 ± 1.4	18.8 ± 1.3	44.4 ± 1.4
−0.15	−0.2	15.3 ± 1.1	12.1 ± 1.0	27.5 ± 1.1
−0.2	−0.25	12.9 ± 1.0	5.93 ± 0.87	18.87 ± 0.94
−0.25	−0.3	7.26 ± 0.78	5.53 ± 0.75	12.80 ± 0.80
−0.3	−0.4	5.18 ± 0.58	2.33 ± 0.54	7.51 ± 0.46
−0.4	−0.5	2.06 ± 0.33	0.95 ± 0.28	3.01 ± 0.32
−0.5	−0.6	1.75 ± 0.33	0.80 ± 0.27	2.55 ± 0.34
−0.6	−0.8	0.59 ± 0.17	0.55 ± 0.18	1.15 ± 0.19
−0.8	−1.0	0.49 ± 0.21	0.87 ± 0.25	1.35 ± 0.25

TABLE II. The results of fits to the differential cross sections in the t' range 0 to -0.4 $(\mathrm{GeV}/c)^2$ of the form $d\sigma/dt = Ae^{bt'}$. The errors given in the table are statistical uncertainties only. A scale uncertainty of ±10% applies to the A coefficients. Also given are the ratio of the cross sections for reactions (1) and (2) at $t = 0$ and at $t' = 0$ obtained by extrapolating the fits.

π^- momentum	8 GeV/c	10.7 GeV/c	15.7 GeV/c
$A(\Lambda)$ (μb)	158 ± 4	117 ± 3	70.4 ± 2.3
$b(\Lambda)$ [$(\mathrm{GeV}/c)^{-2}$]	7.17 ± 0.23	7.85 ± 0.18	7.97 ± 0.19
$A(\Sigma^0)$ (μb)	145 ± 4	103 ± 3	64.5 ± 2.7
$b(\Sigma^0)$ [$(\mathrm{GeV}/c)^{-2}$]	9.16 ± 0.32	9.38 ± 0.24	9.69 ± 0.24
$A(\Lambda+\Sigma^0)$ (μb)	299 ± 5	218 ± 3	133.8 ± 2.5
$b(\Lambda+\Sigma^0)$ [$(\mathrm{GeV}/c)^{-2}$]	7.98 ± 0.19	8.48 ± 0.15	8.67 ± 0.15
$t_{\min}(\Lambda)$ [$(\mathrm{GeV}/c)^2$]	−0.0060	−0.0042	−0.0029
$t_{\min}(\Lambda)$ [$(\mathrm{GeV}/c)^2$]	−0.0089	−0.0064	−0.0044
$[d\sigma/dt(\Lambda)/d\sigma/dt(\Sigma^0)]_{t=0}$	1.05 ± 0.10	1.11 ± 0.10	1.07 ± 0.15
$[d\sigma/dt(\Lambda)/d\sigma/dt(\Sigma^0)]_{t'=0}$	1.09 ± 0.10	1.14 ± 0.10	1.09 ± 0.15

IV. DISCUSSION OF RESULTS

A. Differential and Total Cross Sections

The differential cross sections seem to follow a simple exponential fall from the forward direction out to a break at about $t' = -0.4$ to -0.5 $(\mathrm{GeV}/c)^2$. A maximum-likelihood fit to the form $d\sigma/dt = Ae^{bt'}$ was performed for the data with -0.4 $(\mathrm{GeV}/c)^2 \leq t' \leq 0$; the fitted parameters are given in Table II and the fits shown as the solid lines in Figs. 9–12. At all momenta the forward peak is narrower for reaction (2) than for reaction (1). These fits were extrapolated to yield the ratio of reaction (1) to reaction (2) at $t = 0$ and at $t' = 0$ since both quantities have appeared in the literature. The errors on the ratios are the result of adding the estimated

TABLE III. Total cross sections in μb for reactions (1) $(\pi^- p \to K^0\Lambda)$ and (2) $(\pi^- p \to K^0\Sigma^0)$ and the sum for the t' range 0 to -1.0 $(\mathrm{GeV}/c)^2$. Also given are the ratio of reaction (1) and (2). The errors on the total cross sections are dominated by the 10% systematic uncertainty.

π^- momentum	8 GeV/c	10.7 GeV/c	15.7 GeV/c
$\sigma_{\mathrm{tot}}(\Lambda)$ (μb)	22.1 ± 2.2	15.7 ± 1.6	9.1 ± 1.3
$\sigma_{\mathrm{tot}}(\Sigma^0)$ (μb)	16.7 ± 1.7	11.0 ± 1.1	7.0 ± 1.0
$\sigma_{\mathrm{tot}}(\Lambda+\Sigma^0)$ (μb)	38.8 ± 3.9	26.8 ± 2.7	16.0 ± 1.6
$\sigma_{\mathrm{tot}}(\Lambda)/\sigma_{\mathrm{tot}}(\Sigma)$	1.27 ± 0.04	1.31 ± 0.04	1.33 ± 0.20

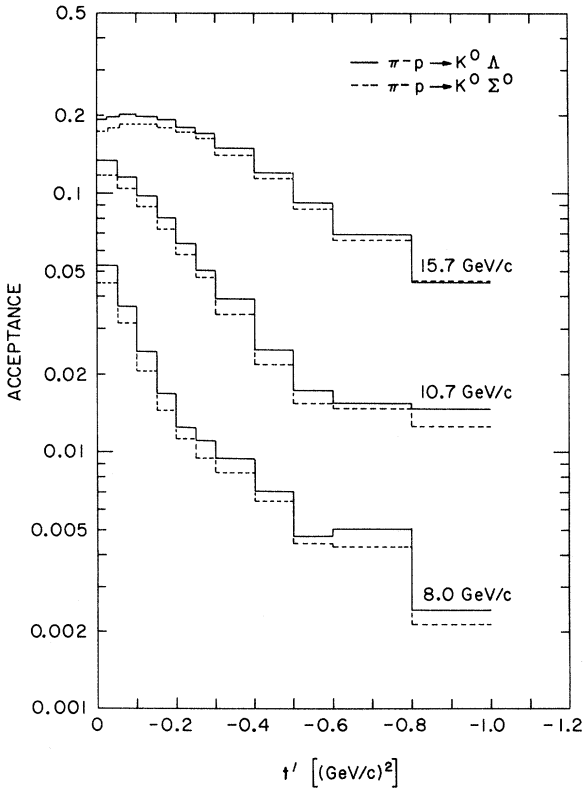

FIG. 8. Apparatus acceptance for events from the reactions $\pi^- p \to K^0\Lambda$ and $\pi^- p \to K^0\Sigma^0$ (solid and dashed lines, respectively) for this experiment.

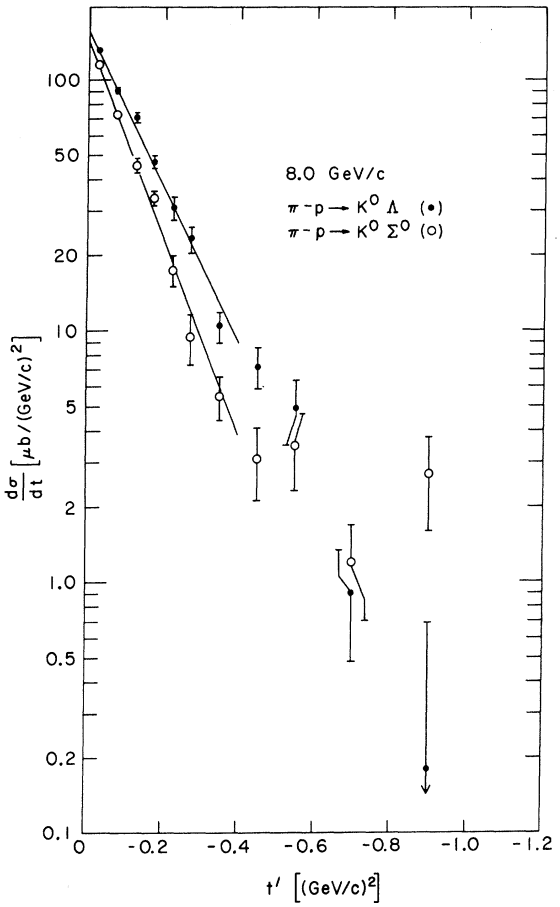

FIG. 9. Differential cross section for $\pi^- p \to K^0 \Lambda$ and $\pi^- p \to K^0 \Sigma^0$ at 8 GeV/c. In addition to the errors shown, there is an absolute scale uncertainty of ± 10% as described in the text. The straight lines are exponential fits to the data between $t' = 0$ and $t' = -0.4$ (GeV/c)^2.

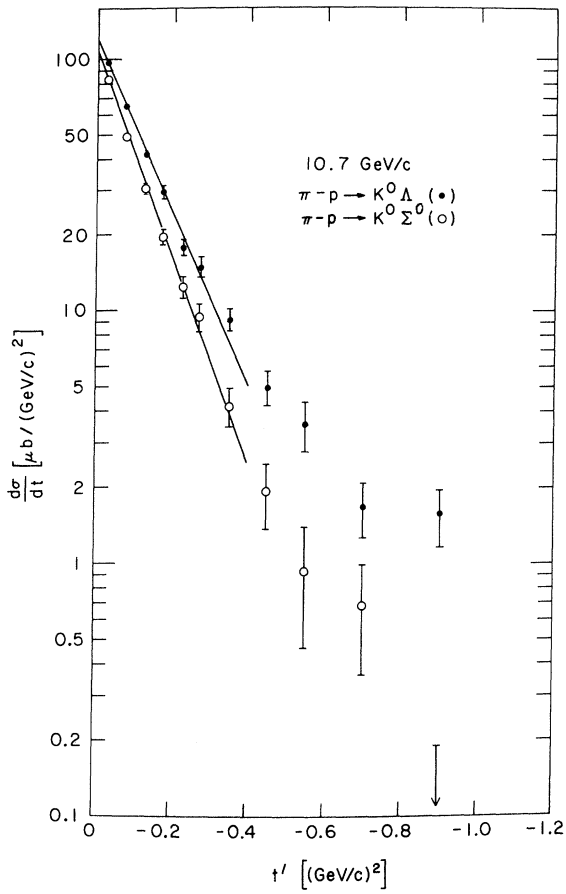

FIG. 10. Differential cross section for $\pi^- p \to K^0 \Lambda$ and $\pi^- p \to K^0 \Sigma^0$ at 10.7 GeV/c. In addition to the errors shown, there is an absolute scale uncertainty of ± 10% as described in the text. The straight lines are exponential fits to the data between $t' = 0$ and $t' = -0.4$ (GeV/c)^2.

systematic uncertainty in the individual acceptance calculations at small t to the statistical errors in the A coefficients, allowing some additional error for the difficulty of separating the reactions at 15.7 GeV/c.

The cross sections in Table I were summed to give the total cross sections [integrated to $t' = -1.0$ (GeV/c)^2] shown in Table III and Fig. 13. The statistical uncertainty in these cross sections is dominated by the systematic uncertainty detailed in Sec. III G. Figure 13 also shows the results of earlier measurements above 3 GeV/c. The lines on Fig. 13 are least-squares fits of the form $\sigma_{tot} \propto p^{-n}$. Although the measurements of Bertolucci *et al.*[2] are systematically lower than this measurement by about 30%, the power law clearly gives a good representation of the data from 3 GeV/c to 15.7 GeV/c. The fitted p dependence of the cross sections is $n = 1.41 \pm 0.06$ for reaction (1), 1.20 ± 0.07 for reaction (2), and 1.43 ± 0.06 for the combined cross section. The fit to the combined cross sections includes data from experiments which do not separate the reactions. The corresponding numbers for this experiment alone are 1.32 ± 0.10 for (1), 1.29 ± 0.11 for (2), and 1.31 ± 0.10 for the sum, the errors in this case being based on the estimated 5% momentum-dependent normalization error.

B. Comparison with $\pi^+ p \to K^+ \Sigma^+$

Isospin conservation predicts that

$$2\frac{d\sigma}{dt}(\pi^- p \to K^0 \Sigma^0) = \frac{d\sigma}{dt}(\pi^+ p \to K^+ \Sigma^+),$$

since it has been shown[9] that the cross section $\pi^- p \to K^+ \Sigma^-$ is very small. In Fig. 14 we have plotted $2d\sigma/dt$ for reaction (2) at 10.7 GeV/c. In

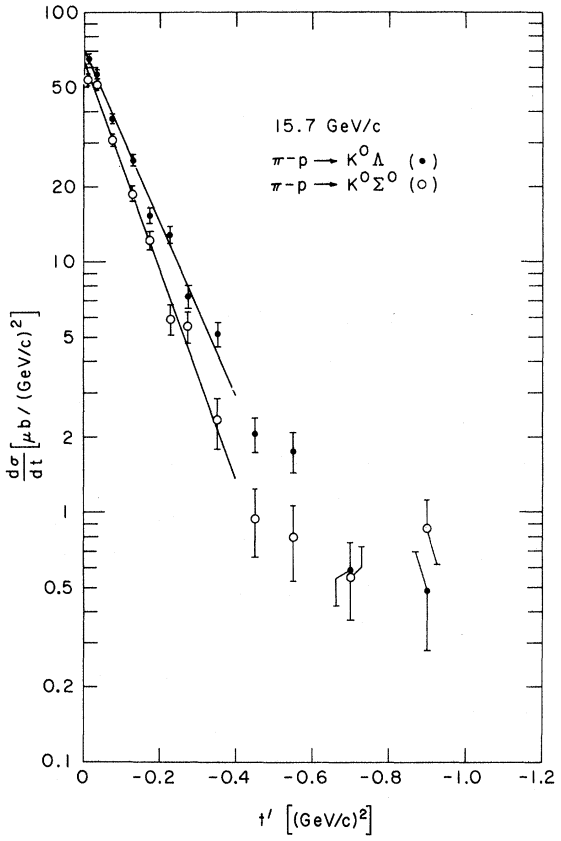

FIG. 11. Differential cross section for $\pi^- p \rightarrow K^0 \Lambda$ and $\pi^- p \rightarrow K^0 \Sigma^0$ at 15.7 GeV/c. In addition to the errors shown, there is an absolute scale uncertainty of ± 15% as described in the text. The straight lines are exponential fits to the data between $t' = 0$ and $t' = -0.4$ $(GeV/c)^2$.

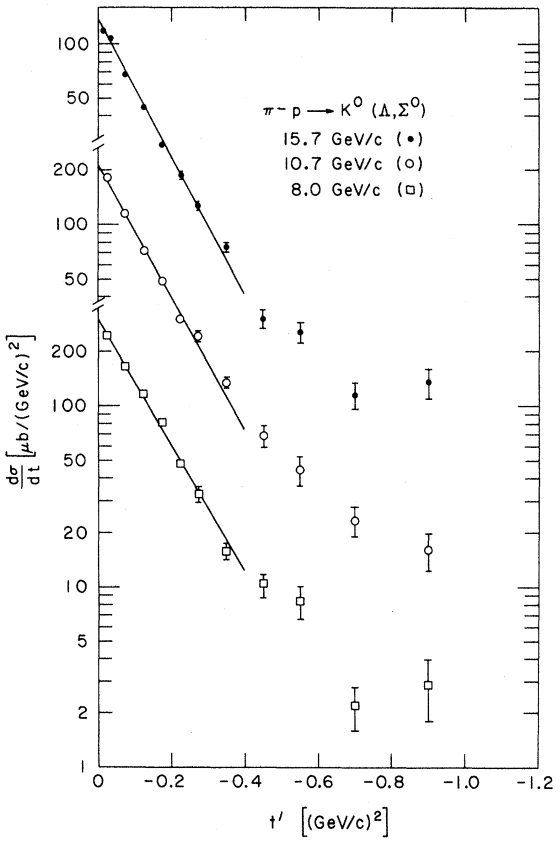

FIG. 12. Combined differential cross section for $\pi^- p \rightarrow K^0 \Lambda$ and $\pi^- p \rightarrow K^0 \Sigma^0$ at 8, 10.7 and 15.7 GeV/c. The systematic scale uncertainty of ± 10% applies to these data.

addition, we have plotted

$$\left(\frac{10.7}{p_{\text{lab}}}\right)^n \frac{d\sigma}{dt}(\pi^+ p \rightarrow K^+ \Sigma^+)$$

on the same figure. Here the factor $(10.7/p_{\text{lab}})^n$ was used to extrapolate the 7-GeV/c data of Ref. 10 and the 10-GeV/c data of Ref. 11. The value of $n = 1.29$ determined by the fit to our measurements of the total cross section for reaction (2) was used. From the figure it can be seen that within normalization errors, the test is well satisfied. The agreement of the 8- and 15.7-GeV/c measurements with extrapolations of the measurements of Refs. 10 and 11 is also adequate, considering the normalization errors.

C. Effective Regge Trajectories

In Fig. 15 we show the differential cross sections $d\sigma(s,t)/dt$ at several values of t for reactions (1) and (2) combined. Here s is the square of the $\pi^- p$ c.m. energy in GeV^2. We can see that the data are fitted well by a straight line as a function of $\ln(s)$. Assuming an equivalent single-Regge-pole form of the s dependence of the type $s^{2\alpha(t)-2}$, where $\alpha(t)$ is assumed to have the simple form

$$\alpha(t) = \alpha(0) + \alpha'(0)t,$$

we obtained fits for $\alpha(0)$ and $\alpha'(0)$ for reactions (1) and (2) separately, as well as the sum of the two. These results are given in Table IV and shown as solid lines in Fig. 16. An estimated 5% momentum-dependent error was compounded with the statistical errors for this analysis.

V. SUMMARY

The measurements of reactions (1) and (2) indicate that the t dependence of the forward peak is fitted by an exponential out to $t' \sim -0.4$ $(GeV/c)^2$ and that the exponential slope of reaction (2) is significantly steeper than reaction (1) up to 15.7 GeV/c. The ratio of the forward differential cross

sections is about 1.1, which is smaller than that measured at lower energies.[1]

The total cross section is falling at about the rate of $p^{-3/2}$ for the combined reactions, with reaction (2) falling somewhat less rapidly than reaction (1).

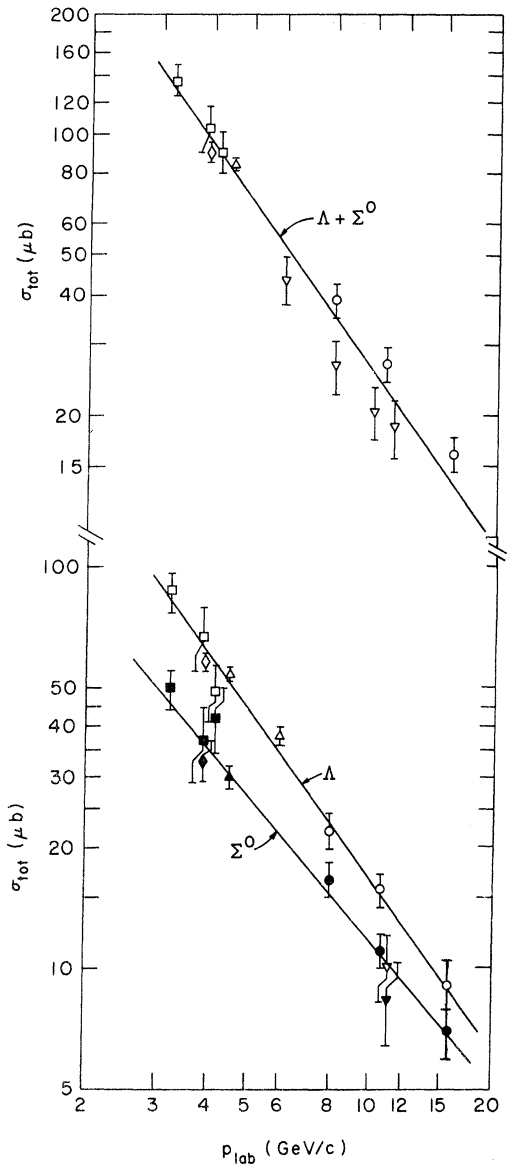

FIG. 13. Total cross section for $\pi^- p \to K^0\Lambda$ and $\pi^- p \to K^0\Sigma^0$. Included are data from Dahl *et al.* (□), Abramovich *et al.* (◇), Crennell *et al.* (△) (all Ref. 1); Bertolucci *et al.*, (▽) (Ref. 2); and this experiment, ○. The solid symbols are for reaction (2). For this experiment σ_{tot} is integrated from $t' = 0$ to -1.0 (GeV/c)^2 and the errors shown are the result of compounding the statistical errors with the systematic scale uncertainties discussed in Sec. III G.

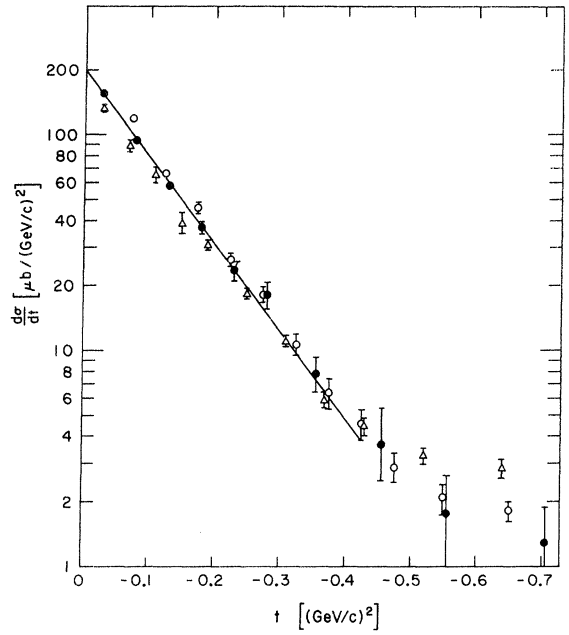

FIG. 14. Comparison of twice the differential cross section for $\pi^- p \to K^0\Sigma^0$ at 10.7 GeV/c (●, this experiment) with the extrapolations to the same momentum of the differential cross sections for $\pi^+ p \to K^+\Sigma^+$ at 7 GeV/c (△, Ref. 10) and 10 GeV/c (○, Ref. 11). The extrapolation procedure is explained in the text.

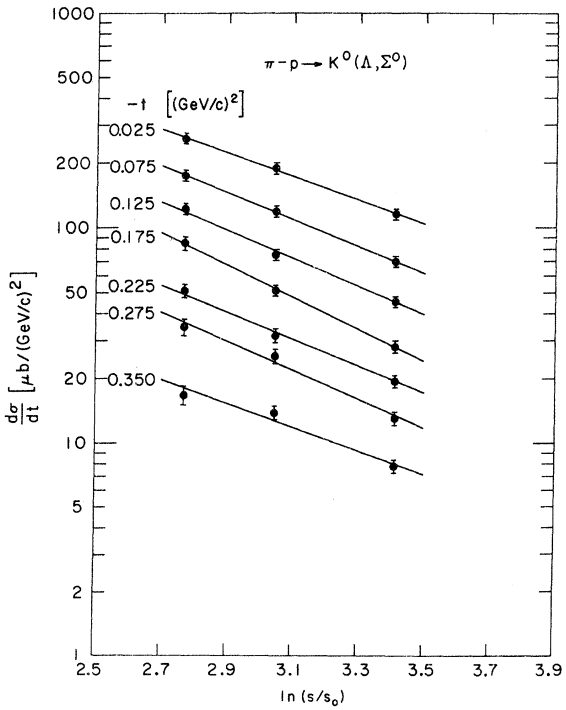

FIG. 15. Differential cross sections at fixed t plotted versus $\ln(s/1\ \text{GeV}^2)$ for the sum of reactions (1) and (2).

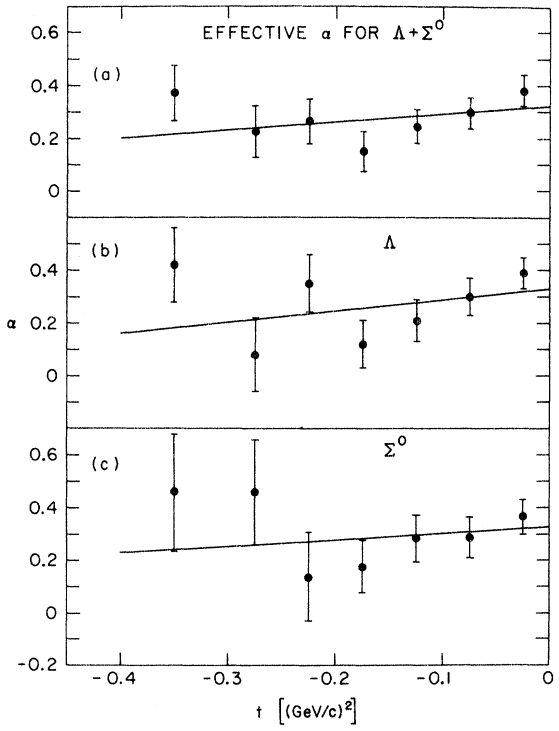

FIG. 16. Effective Regge-pole trajectory α versus t for: (a) the sum of reactions (1) and (2); (b) reaction (1); (c) reaction (2). The solid lines are fits to $\alpha(t)$ as discussed in the text.

TABLE IV. Parameters for linear fits to the effective Regge trajectories for the data of this experiment. A 5% momentum-dependent systematic error was compounded with the statistical error for this fit.

Reaction	$\alpha(0)$	$\alpha'(0)$ [$(\mathrm{GeV}/c)^{-2}$]
$\pi^- p \to K^0\Lambda/\Sigma^0$	0.32 ± 0.05	0.31 ± 0.29
$\pi^- p \to K^0\Lambda$	0.33 ± 0.06	0.43 ± 0.36
$\pi^- p \to K^0\Sigma^0$	0.33 ± 0.06	0.23 ± 0.46

ACKNOWLEDGMENTS

We wish to thank the members of the AGS and EP&S Divisions of the Accelerator Department of Brookhaven National Laboratory for their help in the execution of this experiment. We thank our group technicians for their extended and valuable efforts in the construction and operation of the spectrometer. We acknowledge with thanks the aid and cooperation of the staff of the BNL On-Line Data Facility during the course of this experiment. We express our appreciation to Dr. David Cheng for his assistance with the programming in the early stages of this experiment.

*This work was performed under the auspices of the U. S. Atomic Energy Commission.

[1]O. I. Dahl, L. M. Hardy, R. I. Hess, J. Kirz, D. H. Miller, and J. A. Schwartz, Phys. Rev. 163, 1430 (1967); M. Abramovich, H. Blumenfeld, V. Chaloupka, S. U. Chung, J. Diaz, L. Montanet, J. Pernegr, S. Reucroft, J. Rubio, and B. Sadoulet, Nucl. Phys. B27, 477 (1971); D. J. Crennell, H. A. Gordon, K. W. Lai, and J. M. Scarr, Phys. Rev. D 6, 1220 (1972). References to earlier measurements are found in these papers.

[2]E. Bertolucci, I. Mannelli, G. Pierazzini, A. Scribano, F. Sergiampietri, M. L. Vincelli, C. Caverzasio, J. P. Guillaud, L. Holloway, and M. Yvert, Nuovo Cimento Lett. 2, 149 (1969).

[3]Ph. Salin, Nucl. Phys. B3, 323 (1967); D. D. Reeder and K. V. L. Sarma, Phys. Rev. 172, 1566 (1968); R. D. Field Jr., Phys. Rev. D 5, 86 (1972).

[4]S. Ozaki, D. Cheng, K. J. Foley, S. J. Lindenbaum, W. A. Love, E. D. Platner, A. C. Saulys, and E. H. Willen, in *High Energy Physics*, proceedings of the Fifteenth International Conference on High Energy Physics, Kiev, 1970, edited by V. Shelest (Naukova Dumka, Kiev, U.S.S.R., 1972); E. H. Willen, K. J. Foley, M. A. Kramer, W. A. Love, S. Ozaki, E. D. Platner, A. C. Saulys, and S. J. Lindenbaum, in *Proceedings of the Fourth International Conference on High Energy Collisions*, edited by J. R. Smith (Rutherford High Energy Laboratory, Chilton, Didcot, Berkshire, England, 1972), Vol. 2, pp. 1-24.

[5]K. J. Foley, S. J. Lindenbaum, W. A. Love, S. Ozaki, E. D. Platner, A. C. Saulys, and E. H. Willen, Nucl. Instrum. Methods 108, 33 (1973).

[6]Constraining the Σ^0 and Λ masses to the established values produced a t-independent change in the Σ^0, Λ ratio of 0.02 at 15.7 GeV/c.

[7]B. J. Blumenfeld, L. M. Lederman, R. L. Cool, and S. L. Segler, Nucl. Instrum. Methods 97, 427 (1971).

[8]In order to estimate this quantity, we saved the coordinates of all the sparks associated with the K^0 tracks from an event and used them to replace the K^0 coordinates in the list of sparks for another trigger. The event-processing program was given this new list of sparks and, if it failed to find the K^0 vertex in its new environment, this was treated as an inefficiency of the system. The measurement was made for several complete runs at each momentum. Losses were due to confusion caused by background sparks and out-of-time tracks and distortion of tracks due to the proximity of other sparks. The spark-chamber readout system was limited to eight encodings per magnetostrictive line and so losses occurred if there were more than eight sparks in a gap. See Ref. 5 for a more detailed discussion of this correction. Since the angular distribution of the two pions is determined largely by the decay of the K^0, we estimate that any point-to-point uncertainty in the cross

sections from this inefficiency is smaller than the statistical errors on the points.

[9]C. W. Akerlof, P. K. Caldwell, C. T. Coffin, P. Kalbaci, D. I. Meyer, P. Schmueser, and K. C. Stanfield, Phys. Rev. Lett. 27, 539 (1971).

[10]S. M. Pruss, C. W. Akerlof, D. I. Meyer, S. P. Ying, J. Lales, R. A. Lundy, D. R. Rust, C. E. W. Ward, and D. D. Yovanovitch, Phys. Rev. Lett. 23, 189 (1969); P. Kalbaci, C. W. Akerlof, P. K. Caldwell, C. T. Coffin, D. I. Meyer, P. Schmueser, and K. C. Stanfield, Phys. Rev. Lett. 27, 74 (1971).

[11]A. Bashian, G. Finocchiaro, M. L. Good, P. D. Grannis, O. Guisan, J. Kirz, Y. Y. Lee, R. Pittman, G. C. Fischer, and D. D. Reeder, Phys. Rev. D 4, 2667 (1971).

PHYSICAL REVIEW D VOLUME 8, NUMBER 1 1 JULY 1973

K^+n Charge Exchange at 3.8 GeV/c *

W. Moninger II,† B. Eisenstein, J. Kim, D. Marshall, T. A. O'Halloran, M. Robinson,‡ and P. F. Schultz

University of Illinois at Urbana-Champaign, Urbana, Illinois 61801

(Received 3 August 1972)

We have found 431 events of the reaction $K^+d \to K^0pp_s$ at 3.8-GeV/c K^+ beam momentum in a 295 000-frame exposure of the Argonne National Laboratory 30-in. deuterium-filled bubble chamber. The event sample consists of one- and two-prong events with a visible K^0 decaying to $\pi^+\pi^-$ The total and differential cross sections are found after correction for unseen K^0's and for efficiencies in the scanning-measuring-fitting chain. Comparisons of the data are made to an SU(3) sum rule, a Regge model, and data for $K^-p \to \bar{K}^0n$.

I. INTRODUCTION

We present a study of the reaction

$$K^+n \to K^0p \tag{1}$$

at 3.8-GeV/c incident meson momentum. The data for our study consist of 431 examples of the reaction

$$K^+d \to K^0pp_s \tag{2}$$

from a 295 000-frame exposure of the Argonne National Laboratory (ANL) 30-in. deuterium-filled bubble chamber to the 7° -separated meson beam.

Our study consists of a determination of the total and differential cross section for reaction (1) and comparisons to (a) an SU(3) sum rule due to Barger and Cline[1] relating reaction (1) to the other three meson-nucleon $I = 1$ exchange reactions, (b) the predictions of a Regge model due to Rarita and Schwarzschild,[2] and (c) the total and differential cross-section data for the reaction

$$K^-p \to \bar{K}^0n. \tag{3}$$

A more detailed description of some aspects of this work is found in Ref. 3.

II. EXPERIMENTAL PROCEDURE

A. Scanning and Measuring

All one-prong-plus-vee events and all two-prong-plus-vee events with at least one positive stopping track from the primary vertex found in the scanning fiducial volume were measured on the University of Illinois SMP-CSX-1 system. Two thirds of the film was double-scanned, followed by a third scan to remove discrepancies between the two independent scans. The measurements were processed by the Illinois geometric reconstruction and kinematic fitting programs SPACE and ILLFIT. After the first measurement pass, those events that failed to be spatially reconstructed were measured again. Table I shows the final measurement disposition.

Line A of Table I gives the number of events that were measured and were not rejected either by a computer check of vertex location or by the measurers as being outside the fiducial volume. Line B gives the number of events that were reconstructed after any number of measurements (one, two, and in some special cases, three). Line C gives the estimated number of electron pairs in the sample. This correction was necessary because a study of a sample of events that failed to be reconstructed after repeated measurements revealed that many of these events had vees which were consistent with $\gamma \to e^+e^-$ rather than $K^0 \to \pi^+\pi^-$. Such events could not be reconstructed by SPACE because of the zero-degree opening angle between the electrons. In some of these events, curvature and bubble density as observed on the scan table were consistent with decay electrons rather than pions. When extrapolated to the entire 9227 events measured, 443 ± 111 or $(4.8 \pm 1.2)\%$ are expected to contain electron-pair vees. Subtracting this number from the events that failed to be reconstructed gave the number of events that should have been reconstructed, but were not (line D in Table I). Assuming